

Disentangling cathodoluminescence spectra in nanophotonics: particle resonances vs transition radiation

Saskia Fiedler,[†] P. Elli Stamatopoulou,[†] Artyom Assadillayev,^{‡,†} Christian Wolff,[†]
Hiroshi Sugimoto,[¶] Minoru Fujii,[¶] N. Asger Mortensen,^{†,§} Søren Raza,^{*,‡} and
Christos Tserkezis^{*,†}

[†]*Center for Nano Optics, University of Southern Denmark, Campusvej 55, DK-5230
Odense M, Denmark*

[‡]*Department of Physics, Technical University of Denmark, Fysikvej, DK-2800 Kongens
Lyngby, Denmark*

[¶]*Department of Electrical and Electronic Engineering, Kobe University, Rokkodai, Nada,
Kobe 657-8501, Japan*

[§]*Danish Institute for Advanced Study, University of Southern Denmark, Campusvej 55,
DK-5230 Odense M, Denmark*

E-mail: sraz@dtu.dk; ct@mci.sdu.dk

Extinction spectra The optical response of spherical NPs is described accurately through the exact analytic Mie solution,¹ which is based on expanding the incident plane wave and the scattered field into spherical waves, thus allowing for a straightforward decomposition of the optical spectra into multipolar contributions. In Figure S.1 we show the extinction spectra and the corresponding multipolar decomposition (only electric and magnetic dipolar and quadrupolar terms are shown) for the three Si NPs studied in the main text, with

$R = 62$ nm, $R = 75$ nm, and $R = 105$ nm. The permittivity of Si is taken from Green.² In all cases, the contributions from electric/magnetic dipoles (E/MD) and electric/magnetic quadrupoles (E/MQ) is analysed.

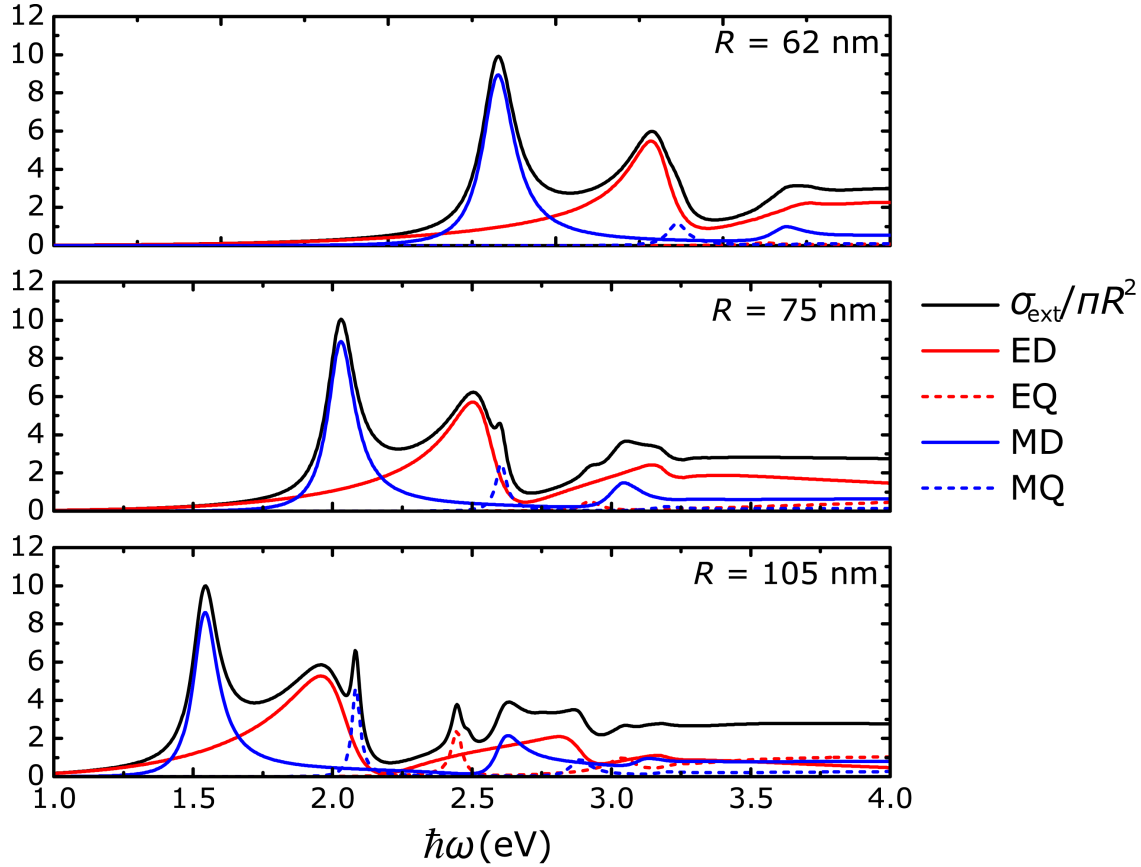


Figure S.1: Mie-theory extinction spectra for the three Si-NP sizes studied in the main text: $R = 62$ nm (upper panel), $R = 75$ nm (middle panel) and $R = 105$ nm (lower panel). Normalised (to the geometrical cross section) extinction is shown in black lines. Red and blue solid and dashed lines correspond to electric and magnetic dipoles and quadrupoles respectively (ED, MD, EQ, MQ).

Analytic CL calculation The analytic theory for the interaction of spherical NPs with fast electron beams has been reported before by García de Abajo.³⁻⁵ In what follows, we provide the analytic expressions for the CL probability. The photon emission probability in the interaction of a dielectric sphere of radius R and relative permittivity (generally dispersive) $\varepsilon(\omega)$ with an electron beam passing along the z axis at distance b (the impact parameter) from the NP centre with constant velocity v is described by the expression⁵

$$\Gamma_{\text{CL}}(\omega) = \frac{e^2}{c\pi\varepsilon_0(\hbar\omega)} \sum_L |\psi_L^{\text{ind}}|^2, \quad (\text{S.1})$$

where e is the elementary charge, c the speed of light in vacuum, ε_0 the vacuum permittivity and $\hbar\omega$ the photon energy. The summation over $L = \{P, l, m\}$ includes electric ($P = E$) and magnetic ($P = M$) multipoles, characterised by the angular momentum numbers l, m , with $l \geq 1$ and $|m| \leq l$. The coefficients ψ_L^{ind} are given by

$$\psi_{Mlm}^{\text{ind}} = \frac{-im}{\sqrt{l(l+1)}} \left\{ A_{lm} K_m \left(\frac{\omega b}{v\gamma} \right) T_l^M + i \int_{-z_0}^{z_0} dz e^{i\omega z/v} Y_l^m(\theta, 0) \left(-k T_l^M h_l^+(kr) + k_1 D_l^M j_l(k_1 r) - k j_l(kr) \right) \right\} \quad (\text{S.2a})$$

$$\psi_{Elm}^{\text{ind}} = \frac{i}{2\sqrt{l(l+1)}} \left\{ \frac{B_{lm}}{\beta\gamma} K_m \left(\frac{\omega b}{v\gamma} \right) T_l^E + \frac{i}{b} \int_{-z_0}^{z_0} dz e^{i\omega z/v} \left(\alpha_l^{-m} \mathcal{I}_{lm}^-(z) + \alpha_l^m \mathcal{I}_{lm}^+(z) \right) \right\}, \quad (\text{S.2b})$$

where

$$\begin{aligned} \mathcal{I}_{lm}^\pm(z) = \mp \left\{ \left[(1 \pm m) Y_l^{m \pm 1}(\theta, 0) \pm \frac{zb}{2(b^2 + z^2)} (\alpha_l^{\pm m + 1} Y_l^{m \pm 2}(\theta, 0) - \alpha_l^{\mp m - 1} Y_l^m(\theta, 0)) \right] \right. \\ \times \left(-T_l^E h_l^+(kr) + D_l^E j_l(k_1 r) - j_l(kr) \right) \\ \left. + \frac{b^2}{\sqrt{b^2 + z^2}} Y_l^{m \pm 1}(\theta, 0) \times \left(-k T_l^E h_l^+(kr) + k_1 D_l^E j_l'(k_1 r) - k j_l'(kr) \right) \right\} \quad (\text{S.3}) \end{aligned}$$

and $\alpha_l^m = \sqrt{(l-m)(l+m+1)}$, $r = \sqrt{b^2 + z^2}$, $\theta = \cos^{-1}(z/r)$, $z_0 = \sqrt{R^2 - b^2}$. In the expressions above, i the imaginary unit, $Y_l^m(\theta, \phi)$ are the usual spherical harmonics of order l, m and polar and azimuthal angles θ and ϕ respectively, K_m the modified Bessel function of the second kind, and j_l, h_l^+ the spherical Bessel and Hankel function of the first kind, respectively, and $j_l', h_l^{+'}$ their derivatives with respect to their argument. The usual relativistic kinematic factors are $\beta = v/c$ and $\gamma = 1/\sqrt{1 - \beta^2}$. The scattering and transmission coefficients read

$$T_l^E = \frac{j_l(k_1 r)[r j_l(kr)]'\varepsilon - j_l(kr)[r j_l(k_1 r)]'}{h_l^+(kr)[r j_l(k_1 r)]' - j_l(k_1 r)[r h_l^+(kr)]'\varepsilon} \Big|_{r=R} \quad (\text{S.4})$$

$$T_l^M = \frac{j_l(k_1 r)[r j_l(kr)]' - j_l(kr)[r j_l(k_1 r)]'}{h_l^+(kr)[r j_l(k_1 r)]' - j_l(k_1 r)[r h_l^+(kr)]'} \Big|_{r=R} \quad (\text{S.5})$$

$$D_l^E = \frac{\varepsilon k h_l^+(k_1 r)[r j_l(k_1 r)]' - j_l(k_1 r)[r h_l^+(k_1 r)]'}{k_1 h_l^+(kr)[r j_l(k_1 r)]' - j_l(k_1 r)[r h_l^+(kr)]'\varepsilon} \Big|_{r=R} \quad (\text{S.6})$$

$$D_l^M = \frac{h_l^+(k_1 r)[r j_l(k_1 r)]' - j_l(k_1 r)[r h_l^+(k_1 r)]'}{h_l^+(kr)[r j_l(k_1 r)]' - j_l(k_1 r)[r h_l^+(kr)]'} \Big|_{r=R} \quad (\text{S.7})$$

The coefficients A_{lm} and B_{lm} entering eqs (S.2) are given by

$$A_{lm} = i^{l+m} \sqrt{\frac{(2l+1)(l-m)!}{\pi(l+m)!} \frac{(2m-1)!!}{(\gamma\beta)^m}} G_{l-m}^{m+\frac{1}{2}} \left(\frac{1}{\beta} \right) \quad (\text{S.8})$$

and

$$B_{lm} = \alpha_l^m A_{l,m+1} - \alpha_l^{-m} A_{l,m-1} \quad (\text{S.9})$$

with $G_{l-m}^{m+\frac{1}{2}}$ denoting the Gegenbauer polynomial.

With these expressions, resonances in the response of an NP are anticipated at the poles of the matrices of eqs (S.4)-(S.7). While eq (S.2b) looks rather complicated, eq (S.2a) provides a clearer picture of the field contributions included in eq (S.1). The field produced by the external part of the electron trajectory and scattered by the particle is accounted for in the first two terms; the third term describes the field generated by the part of the trajectory lying

inside the particle and transmitted to the host environment, and the last term corresponds to the direct field of the electron trajectory, which we disregard by subtracting it from the overall contribution. A more detailed derivation can be found in the Supporting Information of Ref. 5.

Role of Cherenkov radiation Cherenkov radiation (CR) is emitted by a charged particle when moving inside a medium faster than the speed of light in that medium, which translates to the condition $v > c/\sqrt{\epsilon}$.

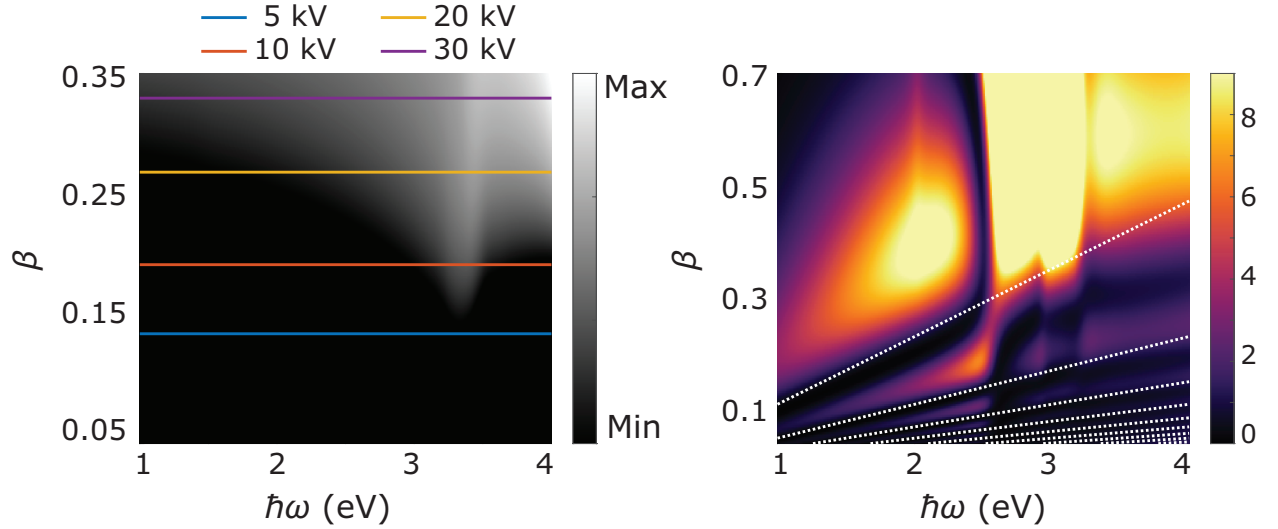


Figure S.2: Contribution of the CR emission in the CL spectra. In the left-hand panel we plot Γ_{CR} as defined in eq S.10, as a function of the photon energy and the electron velocity. The blue, orange, yellow and purple lines correspond to 5, 10, 20, 30 kV acceleration voltage respectively. The right-hand panel is the extended colour map of Figure 3(h) in the main text reaching up to 200 kV, showing the calculated CL spectra, as a function of the electron velocity. Thin white lines serve as guides to the eye for tracing the interference minima.

The shaded area in Figure 3h in the main text shows the energy and electron-beam velocity window lying beyond the CR threshold, where CR emission is possible. In Figures S.2 we show that the CR contribution to the CL signal is practically insignificant for acceleration voltages up to 30 kV, i.e., in the measurements and calculation performed in the present study. For a planar geometry, the CR component of the overall radiation emission

is proportional to the term⁴

$$\Gamma_{\text{CR}} = \left[\frac{1}{c^2} - \frac{1}{v^2 \text{Re}(\varepsilon)} \right]. \quad (\text{S.10})$$

In the left panel of Figures S.2 we plot this term and observe a peak at around 3.3 eV. The blue, orange, yellow and purple lines correspond to 5, 10, 20 and 30 kV acceleration voltage respectively, following the same color-coding as Figures 3g and 4 in the main text. This simplistic approach serves as an indicator of where the CR feature is expected to arise. We note here that, in the experimental measurements, we generally operate in the 1.2 – 3.2 eV energy window.

In the right panel of Figure S.2 we extend the CL color map of Figure 3h to higher acceleration voltages, up to 200 kV ($\beta \approx 0.7$), which is typically used for transmission electron microscopy (TEM) experiments. The CR feature is clearly visible as a broad peak at around 3 eV for $\beta > 0.35$, lying above the destructive interference valleys (white dotted lines) that we discuss in this work.

Monte Carlo simulations Monte Carlo simulations⁶ have been employed to obtain a better understanding of the electron scattering processes within a Si nanosphere at varying accelerating voltages. Exemplary, we show the electron trajectories for a 150 nm-thick Si film on a 15 nm-thin SiN layer, mimicking a Si sphere with $R = 75$ nm —shown as outlines in Figure S.3— as experimentally investigated in Figure 4 in the main text. The blue lines represent the primary electrons and the red ones the back-scattered electrons (BSE). While at low voltage, e.g. 5 kV, the primary and BSE are scattered all over the Si nanosphere, at the highest voltage of 30 kV the electron beam is relatively collimated in the Si layer without any BSE. Ultimately, the higher the acceleration voltage, the “purer” the CL signal, as the incoming electrons are substantially less scattered within the Si sphere, and the time difference between the two collapsing dipoles at the surfaces of the sphere gets shorter. The latter strongly depends on the material thickness and the velocity of the electrons within it.

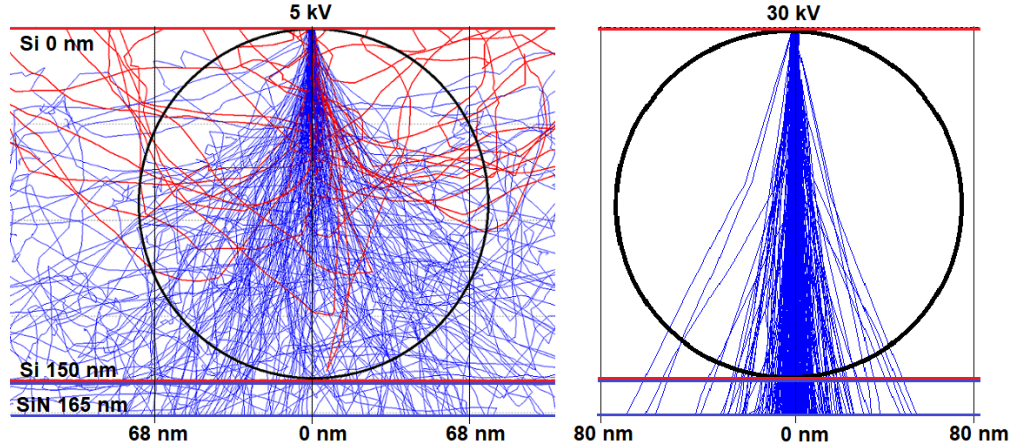


Figure S.3: Monte Carlo simulations of a 150 nm-thick Si layer on a 15 nm-thin Si_3N_4 membrane. To mimic the actual sample, a Si sphere with $R = 75$ nm is exemplary drawn in both panels. The left-hand panel illustrates the electron trajectories of an incoming 5 kV-electron beam, while the right-hand panel displays the trajectories of electrons accelerated at 30 kV. Here, the primary electrons are represented by blue lines and the back-scattered ones by red lines.

Sample degradation test To confirm the stability of the investigated Si nanospheres under long electron-beam exposure, we show in Figure S.4 two 30 kV CL spectra of the same Si sphere ($R = 75$ nm, as studied in Figure 4 in the main text), before and after a series of CL maps collected at varying acceleration voltages. The resulting CL spectra are almost identical—their small differences can be mainly attributed to the experimental challenge of placing the electron beam at the exact same position of the centre of the Si sphere—confirming that spectral changes observed at different voltages do not stem from sample degradation or contamination.

References

- (1) Bohren, C. F.; Huffman, D. R. *Absorption and Scattering of Light by Small Particles*; John Wiley & Sons: New York, Chichester, Brisbane, Toronto, Singapore, 1983.
- (2) Green, M. A. Self-consistent optical parameters of intrinsic silicon at 300 K including temperature coefficients. *Sol. Energy Mater. Sol. Cells* **2008**, *92*, 1305–1310.

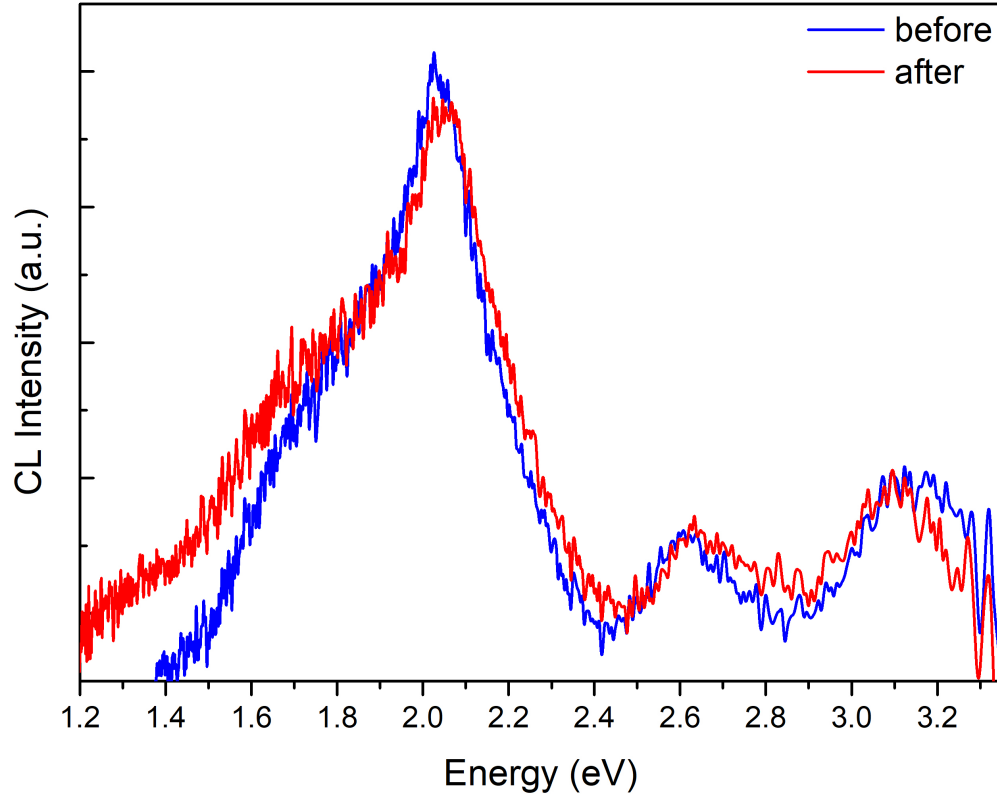


Figure S.4: CL spectra through the centre of the $R = 75$ nm Si sphere of the main text, at acceleration voltage 30 kV, collected at the beginning (blue) and end (red) of the varying acceleration voltage series of Figure 4.

- (3) García de Abajo, F. J. Relativistic energy loss and induced photon emission in the interaction of a dielectric sphere with an external electron beam. *Phys. Rev. B* **1999**, *59*, 3095–3107.
- (4) García de Abajo, F. J. Optical excitations in electron microscopy. *Rev. Mod. Phys.* **2010**, *82*, 209–275.
- (5) Matsukata, T.; García de Abajo, F. J.; Sannomiya, T. Chiral light emission from a sphere revealed by nanoscale relative-phase mapping. *ACS Nano* **2021**, *15*, 2219–2228.
- (6) Drouin, D.; Réal Couture, A.; Joly, D.; Tastet, X.; Aimez, V.; Gauvin, R. CASINO V2.42—A fast and easy-to-use modeling tool for scanning electron microscopy and microanalysis users. *Scanning* **2007**, *29*, 92–101.